

Large Rashba unidirectional magnetoresistance in the Fe/Ge(111) interface statesT. Guillet, A. Marty , C. Vergnaud, and M. Jamet*Université Grenoble Alpes, CEA, CNRS, Grenoble INP, IRIG-SPINTEC, 38000 Grenoble, France*C. Zucchetti  and G. Isella*LNES-Dipartimento di Fisica, Politecnico di Milano, Piazza Leonardo da Vinci 32, 20133 Milano, Italy*Q. Barbedienne, H. Jaffrès , N. Reyren, J.-M. George, and A. Fert *Unité Mixte de Physique, CNRS, Thales, Université Paris-Sud, Université Paris-Saclay, 91767 Palaiseau, France* (Received 31 October 2020; revised 10 January 2021; accepted 27 January 2021; published 5 February 2021)

The structure inversion asymmetry at surfaces and interfaces gives rise to the Rashba spin-orbit interaction (SOI), that breaks the spin degeneracy of surface or interface states. Hence, when an electric current runs through a surface or interface, this Rashba effect generates an effective magnetic field acting on the electron spin. This provides an additional tool to manipulate the spin state in materials such as Si and Ge possessing inversion symmetry in their bulk form. The existence of Rashba states could be demonstrated by photoemission spectroscopy at the interface between different metals and Ge(111) and by spin-charge conversion experiments at the Fe/Ge(111) interface even though it is made of two light elements. In this paper, we identify the fingerprint of the Rashba states at the Fe/Ge(111) interface by magnetotransport measurements in the form of a large unidirectional magnetoresistance of up to 0.1%. From its temperature dependence, we find that the Rashba energy splitting is larger than in pure Ge(111) subsurface states.

DOI: [10.1103/PhysRevB.103.064411](https://doi.org/10.1103/PhysRevB.103.064411)**I. INTRODUCTION**

One of the main promises of spintronics is the implementation of a semiconducting platform where both logic and memory operations could be performed simultaneously, increasing significantly the speed and energy efficiency of such devices [1,2]. Intensive work has been carried out to effectively generate and detect spin accumulations in semiconductors [3–5] and metals [6,7] for the last 20 years. These operations are usually performed using magnetic tunnel junctions in a so-called lateral spin valve geometry [8,9]. This architecture is very close to the prototypical spin transistor originally proposed by Datta and Das in 1990 [10]. In such a structure, the manipulation of spins relies on the Larmor precession by applying an external magnetic field [11], which is incompatible with the very large scale integration paradigm. Therefore, the need for an all-electrical manipulation of the spin orientation is still an ongoing field and is currently stimulating the scientific community.

Recently, we reported the observation of a large unidirectional magnetoresistance (UMR) in the group-IV semiconductor Ge(111) [12]. The detected magnetoresistance exhibits two characteristic features: It is unidirectional and linear with the applied magnetic field and electrical current [13–18]. We showed that this UMR originates from the interplay between an external magnetic field and the Rashba pseudomagnetic field induced by a current passing through the spin-split subsurface states of Ge(111). It is understood as a consequence of the strong spin-orbit interaction (SOI) and is a signature

of the Rashba effect acting on the spins. We also showed that the effect was orders of magnitude stronger than in high SOI systems such as Bi₂Se₃ [13] or SrTiO₃ [15] and could be enhanced or suppressed by applying a gate voltage within a 10 V range.

Although the intrinsic Ge Rashba spin splitting of the subsurface states is not strong enough to target room temperature applications, it can be greatly enhanced at the interface between Ge(111) and metals [19–23]. Hence, beyond providing a way to manipulate the electron spin state, these Rashba states could also be used to generate and detect spin currents in germanium at room temperature, which represents an interesting concept in the field of semiconductor spintronics. In this respect, we previously explored the influence of putting a metal, potentially heavy, in contact with germanium in order to induce and enhance the Rashba SOI [24,25]. In particular, Fe/Ge(111) and Bi/Ge(111) bilayers were extensively studied by a variety of experimental and theoretical techniques. In both systems, we observed spin-charge interconversion at the interface between the two materials due to the presence of Rashba states.

In this paper, we investigate the effect of Rashba states at the Fe/Ge interface on magnetotransport properties. Since Fe and Ge are both conducting materials, the electrical conduction will occur in three parallel channels, exhibiting specific magnetoresistance effects. The Fe thickness was varied from 0 to 3 nm by depositing a wedge of Fe by molecular beam epitaxy (MBE) in order to study the effect of the Fe/Ge interface. The magnitude of the UMR sharply decreases when

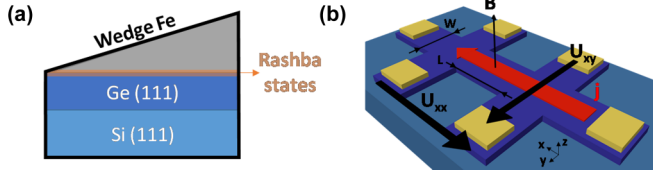


FIG. 1. (a) Illustration of the Fe/Ge/Si(111) wedge sample. (b) Double Hall bar geometry used for electrical measurements.

increasing the Fe thickness as a consequence of the current shunting in the ferromagnetic film. Nonetheless, we managed to observe simultaneously the magnetotransport signatures of the ferromagnetic film and the UMR related to the presence of the Rashba states, which represents a promising observation for applications as one could take advantage of the strong spin polarization of the Rashba states to manipulate the magnetic state of the ferromagnetic (FM) film. Interestingly, when increasing the temperature, the UMR decreases slower than in the case of pure Ge. We could extract a Rashba energy splitting of about $\sim 120k_B$. This value is twice as large as the one obtained in pure Ge(111) ($\sim 60k_B$), indicating that the Rashba SOI is reinforced by the addition of Fe atoms at the Ge(111) surface.

II. SAMPLE PREPARATION

In this study, we use as a substrate a 2- μm -thick Ge/Si(111) film, deposited by low-energy plasma-enhanced chemical vapor deposition (LEPECVD) [26]. The Ge layer is nonintentionally doped with a residual hole carrier concentration $p \approx 2 \times 10^{16} \text{ cm}^{-3}$ as measured by the Hall effect at room temperature [12].

The low p -doped Ge/Si(111) substrate is chemically cleaned with acetone and isopropanol and the native oxide layer is removed using a 50% hydrofluoric acid solution, then loaded into the molecular beam epitaxy (MBE) chamber. A clean Ge (2×8) surface is further obtained by using high temperature annealing and soft argon ion milling cycles in ultrahigh vacuum conditions.

A thickness gradient is obtained by depositing a wedge of Fe at room temperature. The Fe thickness continuously varies from 0 to 3 nm as illustrated in Fig. 1(a). The small lattice mismatch ($\approx 1.3\%$) between Ge and bcc Fe allows the growth of a single crystalline film along the (111) direction [24].

The sample is then patterned into $130 \times 35 \mu\text{m}^2$ Hall bars [Fig. 1(b)] using laser lithography and ion beam etching to define the Fe channel, and Au(120 nm)/Ti(5 nm) ohmic contacts are deposited by e-beam evaporation. An ion-coupled plasma is then employed to etch the 2- μm -thick Ge layer in order to control the current shunting in Ge.

III. CURRENT DISTRIBUTION IN THE Fe/Ge SYSTEM

The temperature dependences of the resistance of three devices with 1.1, 1.7, and 2.3 nm of Fe are reported in Fig. 2(a). They were measured between 10 K and room temperature using a 10 μA AC current at $f = 13.3$ Hz and a lock-in detection. We obtain similar behaviors for the 1.7- and 2.3-nm-thick Fe films: a weak temperature dependence exhibiting a

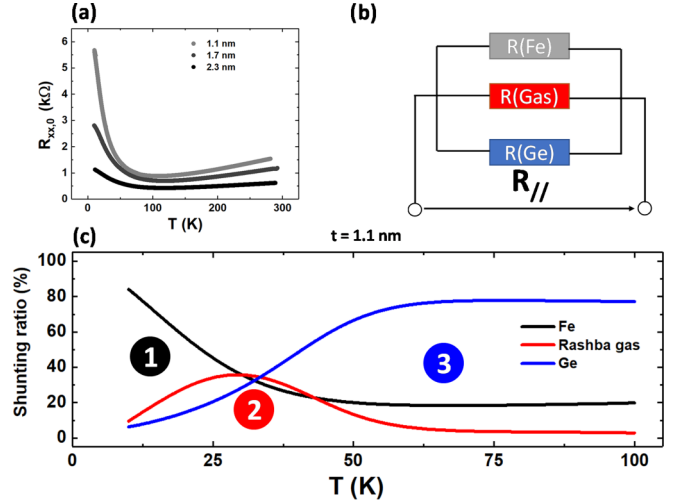


FIG. 2. (a) Temperature dependence of the resistance for different Fe thicknesses. (b) Equivalent electrical resistance of the three channels in the Fe/Ge(111) system. (c) Shunting ratio of the three conduction channels as a function of temperature, extracted from the parallel resistance model presented in Eq. (2).

minimum value. This behavior was also observed in a Fe/MgO (100) reference sample [27]. Interestingly, the 1.1-nm-thick Fe film resistance shows a different temperature dependence. The sharp increase at low temperature seems to indicate that the conduction mostly takes place in the thermally activated Ge channel but the resistance increases linearly (and not exponentially) when decreasing the temperature, suggesting that the transport might occur in a third channel, the interface Rashba gas.

We test this hypothesis by calculating the proportion of the electrical current flowing in the three conduction channels: Ge, Fe, and the Rashba gas [Fig. 2(a)]. The longitudinal zero field resistance $R_{xx,0}$ can be interpreted in the frame of an equivalent parallel resistance as

$$R_{xx,0} = R_{\text{Ge}} \parallel R_{\text{Fe}} \parallel R_{\text{gas}}, \quad (1)$$

where R_{Ge} and R_{Fe} are the resistances of bulk Ge and Fe, respectively, and R_{gas} the resistance of the Rashba gas located at the Fe/Ge interface. The temperature dependences of R_{Ge} and R_{Fe} are recorded on Hall bars sharing the same dimensions as the Fe/Ge (111) one (see Ref. [27]). From these data, we calculate the temperature dependence of R_{gas} and extract the proportion of current shunting γ_i through each of the three channels i from

$$\gamma_i = \frac{G_i}{G_{\text{tot}}}, \quad (2)$$

where i stands for Ge, Fe, or gas, G_i is the conductance of channel i , and $G_{\text{tot}} = G_{\text{Ge}} + G_{\text{Fe}} + G_{\text{gas}}$ the total conductance.

The result of this quantitative analysis is shown in Fig. 2(c), where we see that the conduction mostly occurs in the Ge channel at high temperature and in the Fe film at low temperature. In the intermediate temperature regime, a non-negligible part of the electrical current flows through the third conduction channel which corresponds to the Rashba gas.

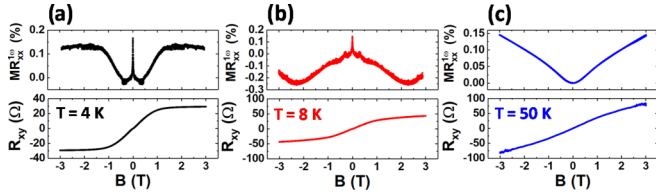


FIG. 3. (a)–(c) 1.1-nm-thick Fe film temperature dependence of the longitudinal magnetoresistance $MR = R_{xx}^{1\omega}(B)/R_{xx}^{1\omega}(B=0)$ (top), and transverse resistance R_{xy} (bottom) using a 10 μA AC current at $f = 13.3$ Hz and a lock-in detection.

To support this interpretation, we performed magnetoresistance (MR) and anomalous Hall effect (AHE) measurements as a function of the sample temperature. The top panels of Fig. 3 show the longitudinal MR curves measured at different temperatures for the 1.1-nm-thick Fe film. The MR is defined as $MR = R_{xx}^{1\omega}(B)/R_{xx}^{1\omega}(B=0)$. At low temperature (4 K), the MR is very weak and shows a saturation behavior, which is the manifestation of the anisotropic magnetoresistance (AMR) and indicates that the transport mostly takes place in the Fe film. In the intermediate temperature range, we observe a W-shaped MR curve which is no longer related to the saturation field of the Fe film and corresponds to the fingerprint of the Rashba MR [28]. At high temperature ($T > 30$ K), the characteristic magnetoresistance of Ge is retrieved as the Ge conductivity increases by the thermal activation of carriers.

The measurements of the transverse resistance R_{xy} [bottom panels in Fig. 3] show a similar behavior: At low temperature, the AHE of Fe is dominant compared to the linear Ge ordinary Hall effect. At higher temperature, the p -type conduction in Ge becomes dominant, as indicated by the positive slope for magnetic fields higher than the saturation field of Fe (≈ 2 T).

Those observations emphasize the result shown in Fig. 2(c), where the proportion the electrical current shunting into each channel is represented. Magnetotransport in Fe/Ge(111) can thus be split into three regimes labeled 1–3 in Fig. 2(c): It is dominated by Fe at low temperature (1), by the Rashba gas at intermediate temperatures (2), and by Ge at high temperature (3). These observations using first harmonic measurements support our assumption that in addition to the semiconducting (Ge) and metallic (Fe) conduction channels, a third channel is present in the system corresponding to the Rashba gas.

IV. ANGULAR-DEPENDENT MEASUREMENTS

In the Fe conduction channel where the SOI is weak, we observe the AMR reported in the top panel of Fig. 3(a). This MR contribution is current independent, and quadratic with respect to the applied magnetic field, i.e., by reversing the field direction, the resistance remains unchanged. However, in the Rashba gas, the SOI results in a current-induced effective field that affects the magnetotransport properties. The resulting magnetoresistance is determined by the relative orientation between the applied field and the current-induced effective Rashba field giving rise to a unidirectional magnetoresistance (UMR) contribution. The complete theoretical description was developed in Ref. [12]. The corresponding symmetries can be easily found by noting that the total magnetic field

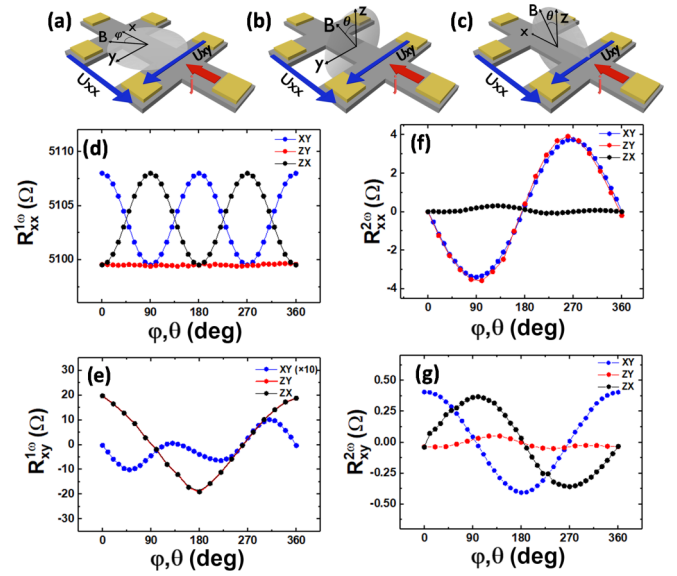


FIG. 4. Angular dependences of the longitudinal and transverse signals in the (a) (xy) , (b) (zy) , and (c) (zx) planes. Corresponding angular dependences of (d) $R_{xx}^{1\omega}$, (e) $R_{xy}^{1\omega}$, (f) $R_{xx}^{2\omega}$, and (g) $R_{xy}^{2\omega}$, measured at 12 K, with an applied magnetic field of 0.5 T and a current of 100 μA .

acting on the carriers is the vector sum of the external field \mathbf{B} and the current-induced Rashba field \mathbf{B}_E . The amplitude of the unidirectional magnetoresistance is expected to be proportional to both the applied magnetic field and the applied current, as the Rashba field is proportional to the current.

In this case, we obtain a resistance term which is linear in current, implying a quadratic dependence of the voltage with the applied current. Since the UMR signals are expected to be rather small due to the current shunting in the Fe layer, we use AC measurements to separate the different harmonics in order to distinguish current-dependent from current-independent resistance contributions. We apply an AC current $I_\omega = I_0 \sin(\omega t)$ and simultaneously record the first and second harmonic longitudinal and transverse resistances: $R_{xx}^{1\omega}$, $R_{xx}^{2\omega}$, $R_{xy}^{1\omega}$, $R_{xy}^{2\omega}$. In addition to this harmonic analysis, we use the magnetic field angular dependences to identify all the magnetoresistance contributions. Figures 4(a)–4(c) illustrate the different measurement geometries. The applied current is along the x direction and the external magnetic field is applied along the (θ, φ) directions, θ and φ being the polar and azimuth angles. The measurements were carried out at 12 K using a 100 μA AC current of frequency $f = 13.3$ Hz, while rotating the sample in the (xy) , (zy) , and (zx) planes in a uniform external field of 0.5 T. Figure 4(d) shows the first harmonic longitudinal resistance $R_{xx}^{1\omega}$ angular dependences measured for the 1.1-nm-thick Fe film. We identify the AMR angular dependence,

$$R_{xx}^{1\omega} = R_{xx}^{1\omega}|_{B_x} + (R_{xx}^{1\omega}|_{B_x} - R_{xx}^{1\omega}|_{B_y}) \sin^2 \theta \sin^2 \varphi, \quad (3)$$

where $R_{xx}^{1\omega}|_{B_x}$ ($R_{xx}^{1\omega}|_{B_y}$) is the longitudinal resistance for the field oriented along the x (y) axis. In the same way, Fig. 4(e) shows the first harmonic transverse resistance $R_{xy}^{1\omega}$ angular dependences measured for the 1.1-nm-thick Fe film. Out-of-plane (zy) and (zx) scans well correspond to the anomalous

Hall effect while the in-plane (xy) angular dependence indicates the presence of the planar Hall effect, the transverse counterpart of the AMR. The external field of 0.5 T is not strong enough to saturate the Fe magnetization, and this results in the V-shaped out-of-plane angular dependence in Fig. 4(e). Overall, this contribution can be expressed as

$$R_{xy}^{1\omega} = R_{\text{AHE}} \cos \theta + R_{\text{PHE}} \sin^2 \theta \sin 2\varphi. \quad (4)$$

Figure 4(f) shows the second harmonic measurements corresponding to the contributions to the resistance that are current dependent [29]. $R_{xx}^{2\omega}$ shows a sine angular dependence with respect to the external field: $R_{xx}^{2\omega}$ changes sign when the external magnetic field is reversed. Regarding the symmetries with respect to the field and current, we call this term unidirectional magnetoresistance (UMR). A similar behavior is observed in the second harmonic transverse measurements $R_{xy}^{2\omega}$ as shown in Fig. 4(g). We define the sine amplitudes as $R_{xx,\Delta}^{2\omega}$ and $R_{xy,\Delta}^{2\omega}$ so that these contributions can be expressed as

$$R_{xx}^{2\omega} = R_{xx,\Delta}^{2\omega} \sin \theta \sin \varphi \quad (5)$$

and

$$R_{xy}^{2\omega} = R_{xy,\Delta}^{2\omega} \sin \theta \cos \varphi. \quad (6)$$

Similarly to the case of pure Ge(111), $R_{xy,\Delta}^{2\omega}$ shows the signature of the Nernst effect, and we can remove this parasitic contribution from $R_{xx,\Delta}^{2\omega}$ by using the following expression [12],

$$R_{\text{UMR}}^{\Delta} = R_{xx,\Delta}^{2\omega} - Z \times R_{xy,\Delta}^{2\omega}, \quad (7)$$

where Z is the aspect ratio of the Hall bar.

In Fig. 5, we report the dependences of R_{UMR}^{Δ} of the 1.1-nm-thick Fe film on the applied current [Fig. 5(a)] and external magnetic field [Fig. 5(b)] (other thicknesses can be found in Ref. [27]). The signal is normalized by the zero field longitudinal resistance $R_{xx,0}$. The UMR is proportional to the current and magnetic field and thus follows the symmetries of the current-induced Rashba field.

We use the figure of merit η which represents the strength of UMR to make a comparison with previous results. It is defined as $\eta = R_{\text{UMR}}^{\Delta}/(R_{xx,0}jB)$ (j being the current density) and represents the strength of the UMR effect. It is interesting to compare the temperature dependence of η of the Fe/Ge(111) systems to the one of bare Ge(111). Figure 5(c) reports the temperature dependence of η , normalized by its maximum value η^{max} . A local maximum is found around 20 K and the effect then sharply decreases with increasing temperature for two reasons: the finite value of the Rashba SOI and the progressive current shunting into the Ge substrate due to carrier thermal activation. Interestingly, the temperature decrease is slightly slower than in pure Ge(111) [12], indicating that the Rashba SOI has been reinforced by the addition of Fe atoms at the Ge(111) surface. To be more quantitative, we define the critical temperature T_R as the temperature at which the slope of η/η^{max} changes. At this temperature, the thermal energy ($k_B T$) becomes larger than the Rashba spin splitting and the UMR effect becomes negligible. We find $T_R \approx 120$ K for Fe/Ge(111) systems which is twice as large as that for

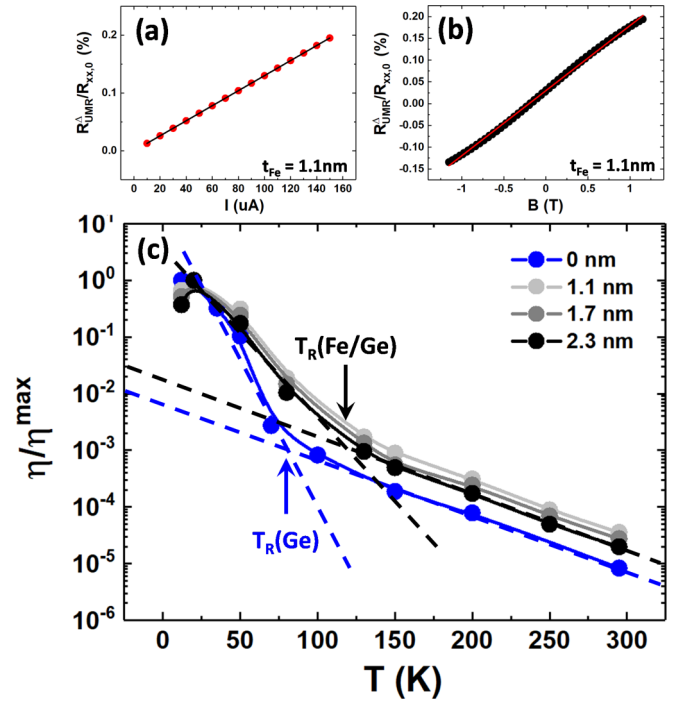


FIG. 5. (a) Current dependence of $R_{\text{UMR}}^{\Delta}/R_{xx,0}$, taken at $B = 0.5$ T and $T = 12$ K for the 1.1-nm-thick Fe film. (b) Magnetic field dependence of $R_{\text{UMR}}^{\Delta}/R_{xx,0}$, taken at $I = 100 \mu\text{A}$ and $T = 12$ K for the 1.1-nm-thick Fe film. (c) Temperature dependence of the figure of merit η defined as $R_{\text{UMR}}^{\Delta}/(R_{xx,0}jB)$, with j being the current density, normalized by its maximum value η^{max} for the 0- [Ge (111) alone, see Ref. [12]], 1.1-, 1.7-, and 2.3-nm-thick Fe films.

bare Ge(111) ($T_R \approx 60$ K), confirming the larger Rashba SOI at the Fe/Ge(111) interface.

At low temperature, the system is equivalent to a bilayer composed of the Rashba gas and the metallic ferromagnet. Therefore, one would expect to detect the unidirectional spin Hall magnetoresistance effect (USMR) [29]: $R_{xx,\text{USMR}}^{2\omega} \propto \mathbf{I} \times \mathbf{M}$. However, this effect is supposed to be two to three orders of magnitude smaller. UMR and USMR effects share the same current and angular dependences, but USMR should follow the Fe magnetization, resulting in the observation of a hysteresis loop at low magnetic field. Figure 5(b) shows that this contribution cannot be resolved in our system using these measurement conditions.

Finally, we present the thickness dependence of $R_{\text{UMR}}^{\Delta}/R_{xx,0}$ (Fig. 6). The measurements were carried out at 12 K, applying an external magnetic field of $B = 0.5$ T and an AC excitation current of $100 \mu\text{A}$. The UMR intensity decreases as the Fe film becomes thicker, and this can be understood since the fraction of the current shunted in the Fe layer becomes larger.

We use the figure of merit η to make a comparison with previous results on different systems. At 15 K, in the 1.1-nm-thick Fe Hall bar, we obtain $\eta = 1.1 \times 10^{-7} \text{ cm}^2/(\text{A T})$ considering that the current completely flows within the spatial extension of the Ge(111) subsurface states (10 atomic layers from Ref. [21]). This value represents a lower bound in this case since a proportion of the current flows in the Fe film. η is four times smaller than in pure p -doped Ge(111)

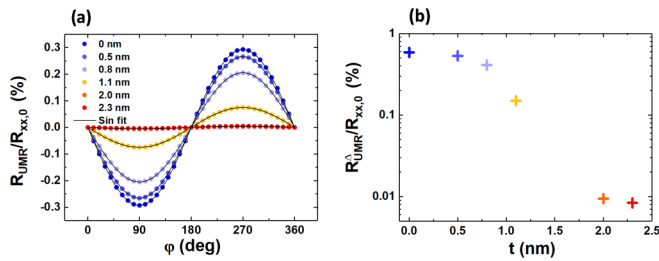


FIG. 6. (a) Angular dependence of the second to first harmonic ratio in the (xy) plane for the different Fe thicknesses measured at 12 K, 0.5 T, and $100 \mu\text{A}$. (b) Corresponding profile for $\varphi = 270^\circ$.

but remains orders of magnitude larger than in other systems reported so far [13,15].

V. CONCLUSION

In conclusion, we measured simultaneously the magnetoresistance contribution from the ferromagnetic Fe layer and the UMR from the Rashba gas at the Fe/Ge(111) interface. Although the amplitude of the UMR is lower than for pure Ge(111), its temperature decay is slower, which is a promising observation for future technological applications at room temperature by selecting the most suitable metal to interface with germanium.

ACKNOWLEDGMENT

The authors acknowledge the financial support from the ANR Project No. ANR-16-CE24-0017 TOP RISE.

- [1] M. T. Bohr and I. A. Young, *IEEE Micro* **37**, 20 (2017).
- [2] S. A. Wolf, D. D. Awschalom, R. A. Buhrman, J. M. Daughton, S. von Molnár, M. L. Roukes, A. Y. Chtchelkanova, and D. M. Treger, *Science* **294**, 1488 (2001).
- [3] O. M. J. van't Erve, A. T. Hanbicki, M. Holub, C. H. Li, C. Awo-Affouda, P. E. Thompson, and B. T. Jonker, *Appl. Phys. Lett.* **91**, 212109 (2007).
- [4] Y. C. Koo, H. Yi, J.-B. Ko, J. Chang, S.-H. Han, D. Jung, S.-G. Huh, and J. Eom, *Appl. Phys. Lett.* **90**, 022101 (2007).
- [5] T. Suzuki, T. Sasaki, T. Oikawa, M. Shiraishi, Y. Suzuki, and K. Noguchi, *Appl. Phys. Express* **4**, 023003 (2011).
- [6] F. J. Jedema, A. T. Filip, and B. J. van Wees, *Nature (London)* **410**, 345 (2001).
- [7] F. J. Jedema, H. B. Heersche, A. T. Filip, J. J. A. Baselmans, and B. J. van Wees, *Nature (London)* **416**, 713 (2002).
- [8] M. Johnson and R. H. Silsbee, *Phys. Rev. Lett.* **55**, 1790 (1985).
- [9] M. Johnson and R. H. Silsbee, *Phys. Rev. B* **37**, 5326 (1988).
- [10] S. Datta and B. Das, *Appl. Phys. Lett.* **56**, 665 (1990).
- [11] J. Fabian, A. Matos-Abiad, C. Ertler, and P. Stano, *Acta Phys. Slovaca* **57**, 565 (2007).
- [12] T. Guillet, C. Zucchetti, Q. Barbedienne, A. Marty, G. Isella, L. Cagnon, C. Vergnaud, H. Jaffrès, N. Reyren, J.-M. George, A. Fert, and M. Jamet, *Phys. Rev. Lett.* **124**, 027201 (2020).
- [13] P. He, S. S.-L. Zhang, D. Zhu, Y. Liu, Y. Wang, J. Yu, G. Vignale, and H. Yang, *Nat. Phys.* **14**, 495 (2018).
- [14] S. S.-L. Zhang and G. Vignale, *Proc. SPIE* **10732**, 1073215 (2018).
- [15] P. He, S. M. Walker, S. S.-L. Zhang, F. Y. Bruno, M. S. Bahramy, J.-M. Lee, R. Ramaswamy, K. Cai, O. Heinonen, G. Vignale, F. Baumberger, and H. Yang, *Phys. Rev. Lett.* **120**, 266802 (2018).
- [16] G. L. J. A. Rikken, J. Fölling, and P. Wyder, *Phys. Rev. Lett.* **87**, 236602 (2001).
- [17] G. L. J. A. Rikken and P. Wyder, *Phys. Rev. Lett.* **94**, 016601 (2005).
- [18] D. C. Vaz, F. Trier, A. Dyrdal, A. Johansson, K. Garcia, A. Barthélémy, I. Mertig, J. Barnas, A. Fert, and M. Bibes, *Phys. Rev. Mater.* **4**, 071001(R) (2020).
- [19] Y. Ohtsubo, S. Hatta, K. Yaji, H. Okuyama, K. Miyamoto, T. Okuda, A. Kimura, H. Namatame, M. Taniguchi, and T. Aruga, *Phys. Rev. B* **82**, 201307(R) (2010).
- [20] Y. Ohtsubo, K. Yaji, S. Hatta, H. Okuyama, and T. Aruga, *Phys. Rev. B* **88**, 245310 (2013).
- [21] T. Aruga, *J. Electron Spectrosc. Relat. Phenom.* **201**, 74 (2015).
- [22] K. Yaji, Y. Ohtsubo, S. Hatta, H. Okuyama, R. Yukawa, I. Matsuda, P. Le Fèvre, F. Bertran, A. Taleb-Ibrahimi, A. Kakizaki, and T. Aruga, *J. Electron Spectrosc. Relat. Phenom.* **201**, 92 (2015).
- [23] C.-H. Lin, T.-R. Chang, R.-Y. Liu, C.-M. Cheng, K.-D. Tsuei, H.-T. Jeng, C.-Y. Mou, I. Matsuda, and S.-J. Tang, *New J. Phys.* **16**, 045003 (2014).
- [24] S. Oyarzún, A. K. Nandy, F. Rortais, J.-C. Rojas-Sánchez, M.-T. Dau, P. Noël, P. Laczowski, S. Pouget, H. Okuno, L. Vila, C. Vergnaud, C. Beigné, A. Marty, J.-P. Attané, S. Gambarelli, J.-M. George, H. Jaffrès, S. Blügel, and M. Jamet, *Nat. Commun.* **7**, 13857 (2016).
- [25] C. Zucchetti, M.-T. Dau, F. Bottegoni, C. Vergnaud, T. Guillet, A. Marty, C. Beigné, S. Gambarelli, A. Picone, A. Calloni, G. Bussetti, A. Brambilla, L. Duó, F. Ciccacci, P. K. Das, J. Fujii, I. Vobornik, M. Finazzi, and M. Jamet, *Phys. Rev. B* **98**, 184418 (2018).
- [26] E. Gatti, F. Isa, D. Chrastina, G. Müller Gubler, F. Pezzoli, E. Grilli, and G. Isella, *J. Appl. Phys.* **116**, 043518 (2014).
- [27] See Supplemental Material at <http://link.aps.org/supplemental/10.1103/PhysRevB.103.064411> for the temperature dependence of the resistance of two reference samples, Fe/MgO and Ge/Si(111), and magnetotransport measurements on two other Fe thicknesses (1.7 and 2.3 nm), which includes Refs. [30,31].
- [28] W. Y. Choi, J. Chang, H.-J. Kim, K.-J. Lee, and Y. C. Koo, *J. Appl. Phys.* **117**, 17C111 (2015).
- [29] C. O. Avci, K. Garello, A. Ghosh, M. Gabureac, S. F. Alvarado, and P. Gambardella, *Nat. Phys.* **11**, 570 (2015).
- [30] S. Sangiao, L. Morellon, G. Simon, J. M. De Teresa, J. A. Pardo, J. Arbiol, and M. R. Ibarra, *Phys. Rev. B* **79**, 014431 (2009).
- [31] C. Liu, Y. Park, and S. D. Bader, *J. Magn. Magn. Mater.* **111**, L225 (1992).